Corrosion Science, 189, (2021), 109575
https://doi.org/10.1016/j.corsci.2021.109575
Accepted 20 May 2021

Significant improvement of the self-protection capability of ultra-high temperature ceramic matrix composites

Francesca Servadei
CNR-ISTEC, Institute of Science and Technology for Ceramics, Via Granarolo 64, I-48018 Faenza, Italy
francesca.servadei@istec.cnr.it

Luca Zoli*
CNR-ISTEC, Institute of Science and Technology for Ceramics, Via Granarolo 64, I-48018 Faenza, Italy
luca.zoli@istec.cnr.it

Antonio Vinci
CNR-ISTEC, Institute of Science and Technology for Ceramics, Via Granarolo 64, I-48018 Faenza, Italy
antonio.vinci@istec.cnr.it

Pietro Galizia
CNR-ISTEC, Institute of Science and Technology for Ceramics, Via Granarolo 64, I-48018 Faenza, Italy
pietro.galizia@istec.cnr.it

Diletta Sciti
CNR-ISTEC, Institute of Science and Technology for Ceramics, Via Granarolo 64, I-48018 Faenza, Italy
diletta.sciti@istec.cnr.it

**Author to whom correspondence should be addressed: luca.zoli@istec.cnr.it*

Abstract

The oxidation behaviour of C_f/ZrB_2-SiC with different fibre architectures, manufactured by slurry impregnation, polymer infiltration and mild pyrolysis, was investigated. Short term oxidation tests in air were performed for 1 min and 5 min at 1500 °C and 1650 °C in a bottom loading furnace. Microstructure, oxide scale thickness and composition were analysed by SEM/EDS/XRD. Results indicated that a good dispersion of ZrB_2 particles in the polymer derived SiC(O) matrix promoted the formation of compact scales filling surface holes left by fibre oxidation. 20-30 vol% of ZrB_2 in the material was found a good compromise between lightness and oxidation resistance.

Keywords: ceramic matrix composites, scanning electron microscopy field-emission, energy dispersive X-ray diffraction, oxidation resistance, surface passivation

1. Introduction

The impelling demand for components able to withstand harsh conditions has been an important driving force for the continuous research of highly performing materials possessing unique properties. Currently used thermal protection systems and rocket motor components of hypersonic space vehicles, satellite launchers (e.g. VEGA, ARIANE) and brake systems of hyper speed vehicles, such as Formula 1 cars, are made of ceramic matrix composites and carbon matrix composites (CMC and CAMCs, respectively). Recently, other sectors such as aviation and metallurgy are replacing refractory metals with CMCs and CAMCs.

On the one hand, carbon/carbon (C/C) composites have excellent high-temperature strength, low CTE and deformability and good thermal shock resistance. On the other hand, they suffer of poor oxidation resistance (above 500 °C) and low wear resistance that reduce their durability and restrict their applications in air at elevated temperatures [1]. Carbon fibre-reinforced silicon carbide (C/SiC) composites possess most of the good properties of C/C composites, and in addition a better oxidation resistance because the diffusion of oxygen can be limited by the formation of a highly viscous film of silica [2,3]. However, the capability to protect carbon fibres is not effective in a wide range of conditions of temperatures and heat fluxes [4–9].

In the past few years, ultra-high temperature ceramics (UHTC), a class of refractory ceramics consisting of borides and carbides of the early transition metals (group IV and V), , have

gained increasing interest as a potential substitute of carbon and silicon carbide ceramic matrices in CMCs owing to their excellent thermal and chemical stabilities [10–13]. Among UHTCs, ZrB_2 is the most investigated UHTC phase [13–15] because of balanced characteristics, such as relative low density (~6 g/cm^3), lower cost compared to HfB_2 and good oxidation and ablation resistance, especially when combined with minor amounts of other ceramic phases, such as SiC [16–18], La_2O_3 [19,20] and $TaSi_2$ [21]. Such multiphase matrices offer a better oxidation resistance and self-healing capability in a wider range of temperatures. For instance, the oxidation of pure ZrB_2 leads to the formation of a porous, solid ZrO_2 layer and a film of liquid B_2O_3, which spreads on the surface and inhibits the inward diffusion of oxygen into the underlying bulk material (slowing fibre oxidation) up to its temperature of vaporization (~1100 °C). Conversely, a ZrB_2 – SiC matrix protect fibres at even higher temperature by forming a borosilicate glass above 1100 °C, which is less viscous than pure silica, spreading better along the surface, sealing cracks and defects but at the same time is more viscous and less volatile than pure B_2O_3 [22]. Moreover above 1600 °C ZrO_2 improves glass durability (solid particles embedded into the glass induce a physical modification) while its partial dissolution promotes a chemical modification of Si-O bonds [23].

Consequently, achieving a homogeneous distribution of ZrB_2 and SiC phases around carbon fibres is the goal for improving material durability. Unfortunately, the phase composition (ceramic phases and carbon fibres) and their distribution in the composite are often the consequence of the manufacturing process selected rather than a study of the material design. Some examples of manufacturing methods and characterization of oxidation resistance of UHTCMCs are reported in Table 1.

Table 1. Main results that have been done in this field of ceramic matrix composites and tests at high temperature to evaluate oxidation resistance.

Techniques	Materials	Fibre (vol%)	UHTC (vol%)	SiC (vol%)	Testing	Authors
PIP, VSI	C/C+ZrB_2-SiC coating	n/a	n/a	n/a	Furnace, 1500 °C, 40 min	Zhou et al. [24]

CVI, PC	C/C+ZrB_2-SiO_2 coating	n/a	n/a	n/a	Furnace, 1500 °C, 330 h	Haibo et al. [25]
CVI	C/C+ZrB_2-SiC coating	n/a	n/a	n/a	Solar furnace, 1700–2600 °C	Corral et al. [26]
CVI	C/SiC-ZrB_2	25	4	71	Electric furnace, 1000–1400 °C, 5 min	Tang et al. [27]
PIP, SI, CVD	C/ZrB_2-SiC	54	n/a	n/a	Blow torch, 3000 °C, 20 s	Liu et al. [28]
SI, HP	C/ZrB_2-SiC	42	52	6	TGA	Vinci et al. [29]
SI, HP	C/ZrB_2-SiC	37	46	12	Furnace, 1500–1650 °C, 1 min	Vinci et al. [30]
SI, HP	C/ZrB_2-SiC	53	26	17	Furnace, 1650 °C, 1 min	Zoli et al. [31]
SI, PIP	C/ZrB_2-SiC	30-31	29-19	35-42	Furnace, 1650 °C, 1 min	Servadei et al. [33]
SI, PIP	C/ZrB_2-SiC	30-31	29-19	35-42	TGA, furnace, 1500–1650 °C, 1-5 min	Present work

PIP: Polymer Infiltration and Pyrolysis.
VSI: Vapour Silicon Infiltration.
CVI: Chemical Vapour Infiltration.
PC: Pack Cementation.
SI: Slurry Infiltration.
CVD: Chemical Vapour Deposition.
HP: Hot Pressing.

Some authors applied an environmental barrier coating (EBC), made of UHTCs, on conventional C/C composites [24–26] and tested the material from 1500 °C to 2600 °C. The adhesion between the composite and the coating could be compromised due to the different chemistry of the materials and the thermal expansion mismatch under severe thermal stresses. Other authors introduced ZrB_2 powders into fibre preforms via slurry impregnation and consolidated the material using non-sintering routes: chemical vapour infiltration (CVI) with methane gas [27], polymer infiltration and pyrolysis (PIP) with polycarbosilane [28,32–34] and sintering approaches: pack cementation (PC) [25] and hot pressing (HP) [29–31].

Recently, we presented a novel two-step, non-sintering, near-net shape route to manufacture lightweight UHTCMCs (densities of 2.7 - 3.2 g/cm^3) containing about 20 - 30 vol% of ZrB_2

(depending on fibre architecture) with homogeneously distributed ZrB_2 and SiC phases around each carbon fibre, even using 2D cloths [32]. Even though the matrix was consolidated under the mild conditions of 1000 °C, passivation occurred within few microns below the material surface after oxidation at 1650 °C for 1 min [32].

Here we presented an extensive study of the oxidation behaviour of the same material via thermo-gravimetric analysis (TGA) up to 1350 °C and short oxidation tests in air at 1500 °C and 1650 °C for 1 min and 5 min. The aim of this work is to highlight that a good dispersion of ZrB_2 particles in the polymer derived SiC(O) matrix is of utmost importance in order to promote a fast passivation of the material.

2. Experimental

2.1 Materials

Commercially available products were used for the preparation of ceramic matrix composites, I) ceramic powders: SiC (Alpha, Grade UF-25, H.C. Starck, Germany; specific surface area 23–26 m^2/g, impurities (wt.%): 2.6 O), ZrB_2 (Grade B, H.C. Starck, Germany; specific surface area 1.0 m^2/g, particle size range 0.5–6 μm, impurities (wt.%): 2 O, 0.25 C, 0.25 N, 0.1 Fe, 0.2 Hf); II) polymeric precursor of SiC (Allyl-hydrido polycarbosilane, StarPCS^{TM} SMP-10, Starfire System Inc., U.S.A.; density 0.998 g/cm^3, viscosity 40–100 cPs at 25 °C) and the cross-linker catalyst (trimethyl(methylcyclopentadienyl)platinum(IV), Sigma Aldrich; purity 98%); III) unidirectional (UF-XN80-300, Granoc, Japan; fabric areal weight 330 g/m^2) and plain woven (PF-XN80-240, Granoc, Japan; areal weight 240 g/m^2) fabrics made of ultra-high modulus pitch-based carbon fibre (XN80-60S, yarn: 6K, diameter 10 μm, density 2.17 g/cm^3, tensile modulus 780 GPa, tensile strength 3.4 GPa).

2.2 Process

Three C_f/ZrB_2-SiC samples with different fibre architectures (Fig. 1), were fabricated by a cycle of water-based slurry infiltration of fibre fabrics, using a mixture of ZrB_2 – 10 vol% SiC

powders, following the procedures previously reported in our paper [31], followed by repetitive cycles of polymer infiltration and pyrolysis. A sample was realized by stacking infiltrated plain woven fabrics (sample labelled as 2D); a second sample, with an asymmetric orientation of fibres, was prepared by stacking unidirectional infiltrated fabrics with the same orientation (sample labelled as 0-0°), while a third sample, with symmetric configuration of fibres, was obtained by stacking unidirectional infiltrated fabrics with 0-90° orientation (sample labelled as 0-90°). Infiltration with SMP-10 (containing 1 wt.% of catalyst) and pyrolysis cycles at 1000 °C under argon flux were carried out six times to reduce the porosity below 10%. Further details are reported in [32].

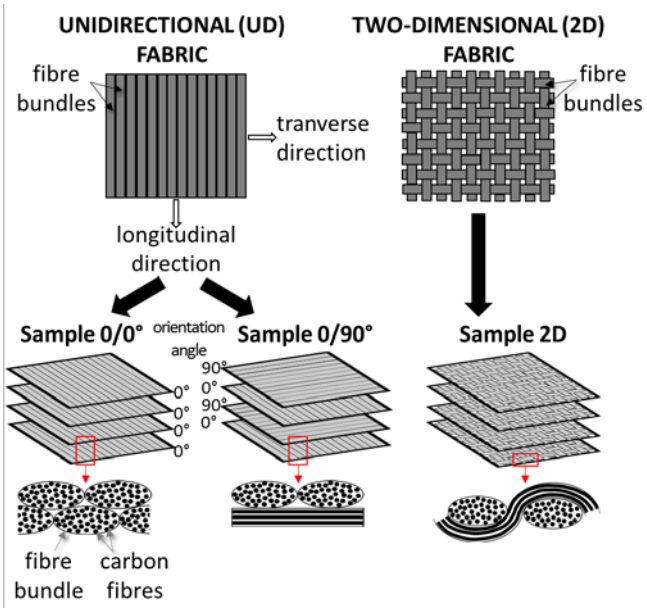

Figure 1. Schematic representation of C_f/ZrB_2-SiC samples with different fibre architectures: sample 0-0°, prepared by stacking infiltrated unidirectional (UD) fabrics with the same orientation, sample 0-90°, prepared by stacking infiltrated UD fabrics with the 0-90° orientation, and sample 2D, realized with infiltrated and subsequently piled up plain woven (2D) fabrics.

2.3 Oxidation tests

Regular samples sized 9 mm × 4 mm × 2 mm were cut from the pellet labelled 0-0°. In order to identify the critical oxidation temperatures, the oxidation test was carried out in a thermogravimetric analyser (STA 449 C Jupiter, NETZSCH, Geraetebau GmbH, Germany), in

synthetic air (composition: 80 vol% N_2 + 20 vol% O_2, with 30 mL/min gas flow), up to 1350 °C with a heating rate of 10 °C/min.

In order to evaluate resistance in extreme environments, short term oxidation tests were carried out in a bottom loading furnace (FC18-0311281, Nannetti S.r.l., Italy) at 1500 °C and 1650 °C in air for 1 min and 5 min on 10 mm × 10 mm × as-processed thickness plates, which were cut from 0-0°, 0-90° and 2D samples. The plates were put on a porous zirconia sample holder, resting on one of the two largest surfaces, and introduced in the furnace when the target temperature was reached. At the end of the oxidation stage, the samples were removed and left to cool naturally in air.

2.4 Characterization

After the pyrolysis cycles, bulk densities were measured by Archimedes' method. Open porosity in the range 0.0058-100 μm was determined by mercury intrusion porosimetry (Pascal 140 and Pascal 240 series, Thermo Finnigan, U.S.A.). The fibre volumetric amount was determined taking into account the number of layers, sample area, the fibre areal weight (g/m^2) and the fibre density given by the supplier. The powder amount in the matrix was calculated as the difference between the weight of the pellet after slurry infiltration (after drying) and fibre weight. The polymer derived ceramic weight was calculated as the difference between pellet weight before and after six PIP cycles. The topological characterization of the surface of the as-obtained samples was performed with a Contour GT-K 3D non-contact profilometer (Bruker, Germany) on 8 mm × 8 mm areas, then the data were analysed using the commercial software Vision64 Map.

Specimens for both oxidation tests were cleaned with ethanol and dried under IR lamp. During TGA test, the mass variation was recorded continuously by the analyser (sensitivity 10^{-3} mg). Specimens for short oxidation tests were weighed with an analytical balance (accuracy ±0.01 mg) before (w_{in}) and after oxidation test (w_{fin}). Mass variation was normalized over the initial surface area using equation: $\frac{\Delta m}{S} = \frac{w_{fin} - w_{in}}{S}$, in which S is the initial surface area, measured by calliper (accuracy ± 0.05 mm). X-ray diffraction analysis was carried out from 10 to 80° (step 0.02, step

time 0.5 s) using an apparatus (D8 Advance, Bruker, Germany) with CuKα radiation and a LYNXEYE detector on air-exposed surface of samples to determine phases after oxidation. The microstructures and elemental composition of the as-processed material and oxidized specimens were analysed using field emission gun-scanning electron microscope (FE-SEM, Carl Zeiss Sigma NTS Gmbh, Germany) and energy dispersive X-ray spectroscopy (EDS, INCA Energy 300, Oxford instruments, UK) on surface and cross-section, to reveal modifications induced by oxidation. Polished specimens for microscopy were prepared by cutting cross sections from tested samples, mounting them in epoxy resin and polishing them using semi-automatic polishing machine (Tegramin-25, Struers, Italy), then washed with ethanol and acetone in an ultrasonic bath. All oxidized samples were coated with a thin layer of carbon using a turbo-pumped sputter coater (Q150T ES, Quorum Technologies Ltd, UK).

3. Results and discussion

3.1 Microstructure of as-obtained materials

In Table 2 the physical properties of samples, unidirectional (UD: 0-0° and 0-90°) and two-dimensional woven (2D), presented in the previous work [32], are shown. Matrix compositions, fibre amounts and porosities were similar for UD samples regardless of fibre orientation on the plane. In the case of 2D sample, a lower amount of ZrB_2 phase, a higher amount of silicon carbide and a higher porosity were found.

Table 2. Bulk density, open porosity and compositions of the as-obtained composites.

Sample label	0-0°	0-90°	2D
Bulk density (g/cm^3)	3.2 ± 0.2	3.2 ± 0.2	2.7 ± 0.3
Open porosity (%)	~6	~6	~9
C_f (vol%)	30 ± 1	31 ± 1	30 ± 1
UHTC (vol%)	29 ± 1	27 ± 1	19 ± 1
SiC (vol%)	35 ± 1	36 ± 1	42 ± 1

Such differences in composition were ascribed to the higher complexity of the 2D fibre architectures compared to the UD ones, which hindered the powder slurry infiltration. Moreover,

the lower powder fraction in the infiltrated fabrics explained the lower UHTC content in the consolidated material, which was offset by a higher content of polymer derived ceramic (PDC). The higher number of defects in the powder/fibre compact was easily reduced by repetitive cycles of PIP due to the use of a higher amount of low viscous SMP-10 [32]. The resulting 2D sample presented a higher roughness than UD samples. In Fig. 2a,b, the optical picture and the roughness profile mapping of the 2D sample were reported. The Fig. 2b shows the shape and depth of four cavities formed at the intersection of the bundles on the external layer, and the 3D surface topography of two cavities were reported in Fig. 2c. Finally, the SEM analysis of the sample cross section highlighted the presence of PDC spots showing shape and size similar to the cavities visible on the sample surface (Fig. 2d).

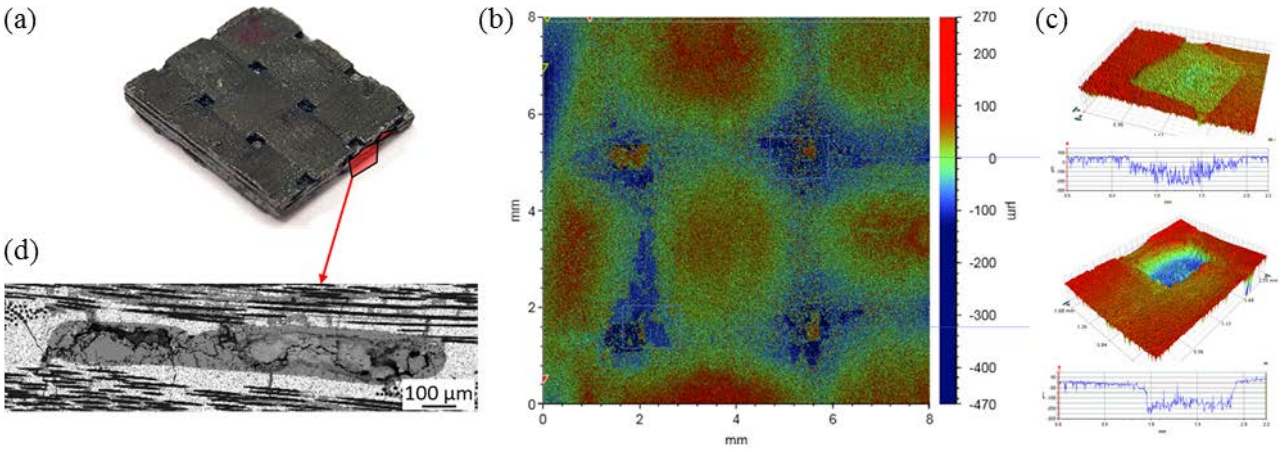

Figure 2. Sample 2D: (a) optical picture, (b) 2D image obtained by laser profilometer, (c) 3D detail of two areas of (b) showing surface topography, (d) back-scattering micrograph of cross section showing a PDC spot (grey colour) in the cross of fibre bundles.

Apart from above mentioned differences in sample compositions and porosities, the microstructures of the three samples were quite similar. An example of microstructure of the cross section of the samples is shown in Fig. 3. Black dots are carbon fibres, the white contrasting phase is ZrB_2, while the grey regions are silicon carbide. Polymer derived ceramic (PDC) SiC was hardly distinguishable from SiC powder particles (Fig. 3) due to the low contrast difference; the former was found either finely dispersed in the ZrB_2 matrix, or in large spots filling the cavities, whereas

SiC powder particles were mainly found homogeneously distributed in the ZrB_2 matrix around the fibres.

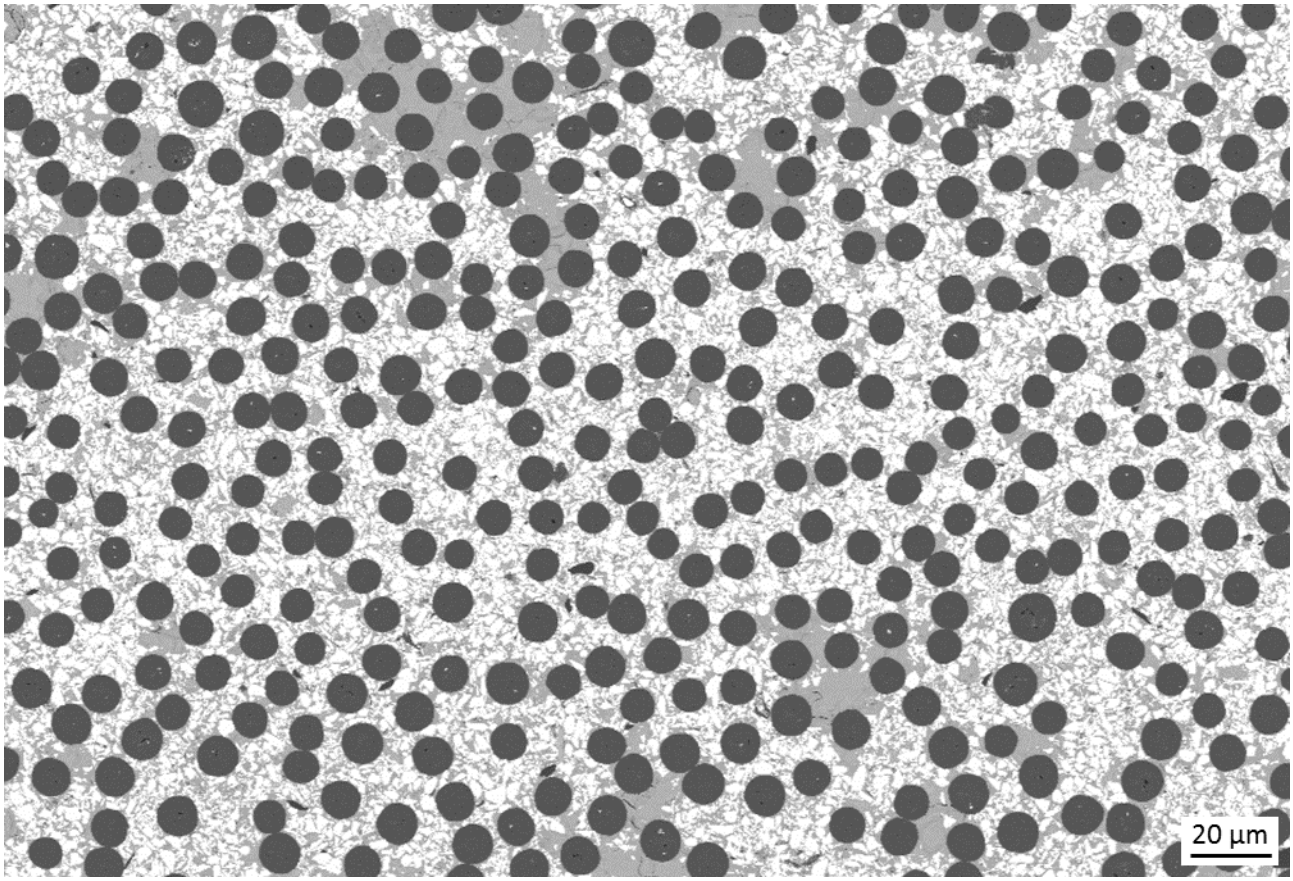

Figure 3. SEM micrograph of the polished section of the 0-0° sample, showing the good homogeneity of carbon fibre (black phase) embedded in ZrB_2 (white phase) – SiC (grey phase) matrix.

3.2 Thermogravimetric analysis

Fig. 4 shows the non-isothermal TG curve up to 1350 °C in air, the critical oxidation temperatures, and the microstructure and chemical composition of the glassy phase.

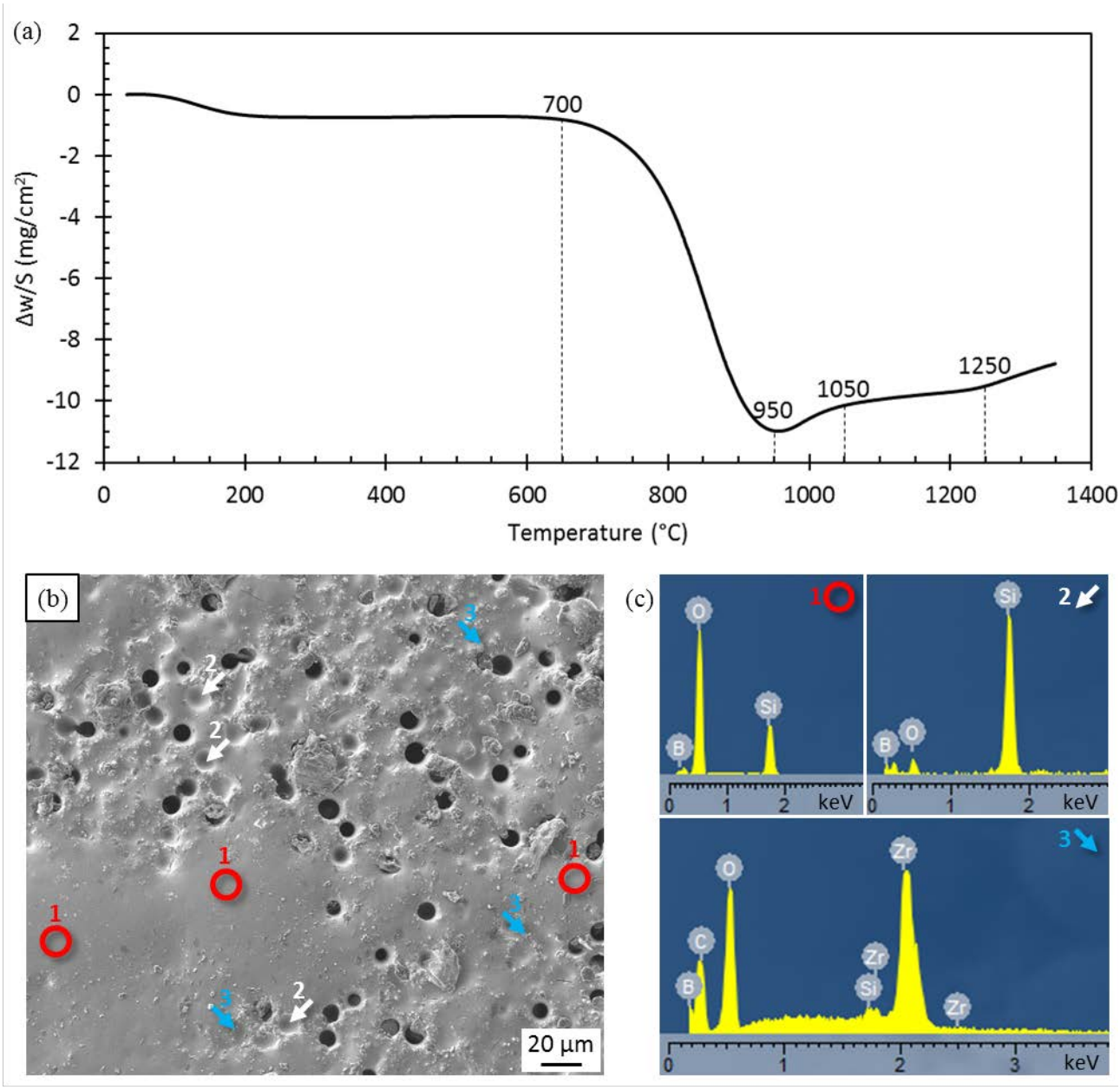

Figure 4. (a) Specific weight change (Δw/S) vs temperature (°C) of the tested material and (b) SEM micrograph of the oxidized surfaces after TGA. (c) EDS spectra (EDS spots were marked in Fig. 3b) of the glassy phase, mainly consisting of boron and silicon oxides with embedded ZrO_2 particles.

Above 700 °C and up to 950 °C a rapid weight loss occurred (Fig. 4a). This was ascribed to the rapid oxidation of the exposed carbon fibres due to the evolution of carbon oxides according to the following reactions:

$$C + 1/2\ O_2 \rightarrow CO \quad (1)$$

$$C + O_2 \rightarrow CO_2 \quad (2)$$

In this range of temperature, the rate of oxidation of ZrB_2, see reaction (3), was not sufficient to balance the weight loss due to fibre oxidation. The passivation mechanism promoted by liquid B_2O_3 was not sufficient to limit O_2-diffusion into the bulk [29].

$$ZrB_2 + 1/2\ O_2 \rightarrow ZrO_2 + B_2O_3 \quad (3)$$

At 950 °C, mass loss came to a halt. This change in the curve was probably due to an increase in oxidation rate of ZrB_2 and formation of a partially effective, self-protective liquid glass layer percolating in the holes left by fibre removal. Beyond 950 °C and up to 1050 °C, mass gain became predominant. In this range of temperatures, the oxidation of polymer derived silicon carbide (pyrolysed at 1000 °C) started to be relevant [35], see reaction (4):

$$SiC + 3/2\ O_2 \rightarrow SiO_2 + CO \quad (4)$$

The slope reduction from 1050 to 1250 °C was attributed to the formation of borosilicate glass, see reaction (5), which is more effective to hinder oxygen diffusion. Above 1250 °C a slight increase in the slope pointed out an increase in the rate of oxidation which was attributed to faster ZrO_2 formation.

$$SiO_2 + B_2O_3 \rightarrow SiO_2{\cdot}B_2O_3 \quad (5)$$

The sample surface after TGA was characterized by a uniform glassy phase covering the majority of the composite, with the presence of partially filled fibre hollows (Fig 4b). The glassy phase mainly consisted of silicon and boron oxides with small zirconia nanoparticles embedded in the glass (Fig 4c).

3.3 Short term oxidation tests

Optical pictures of 0-0°, 0-90° and 2D samples after 1 min and 5 min oxidation tests at 1500 °C and 1650 °C are shown in Fig. 5. After 1 min exposure in air at 1500 °C, the grey colour typical of the as-processed materials acquired a dark blueish tint, sign of borosilicate glass formation, and after 5 min, white spots were visible on the surface, indicating the presence of ZrO_2. The oxidized samples at 1650 °C for 1 min appeared the most damaged of the series, showing flakes of silica;

nevertheless the original shape was preserved, while after 5 min exposure, a soft bubble of iridescent glass was formed on the surface of the samples (Fig. 5d).

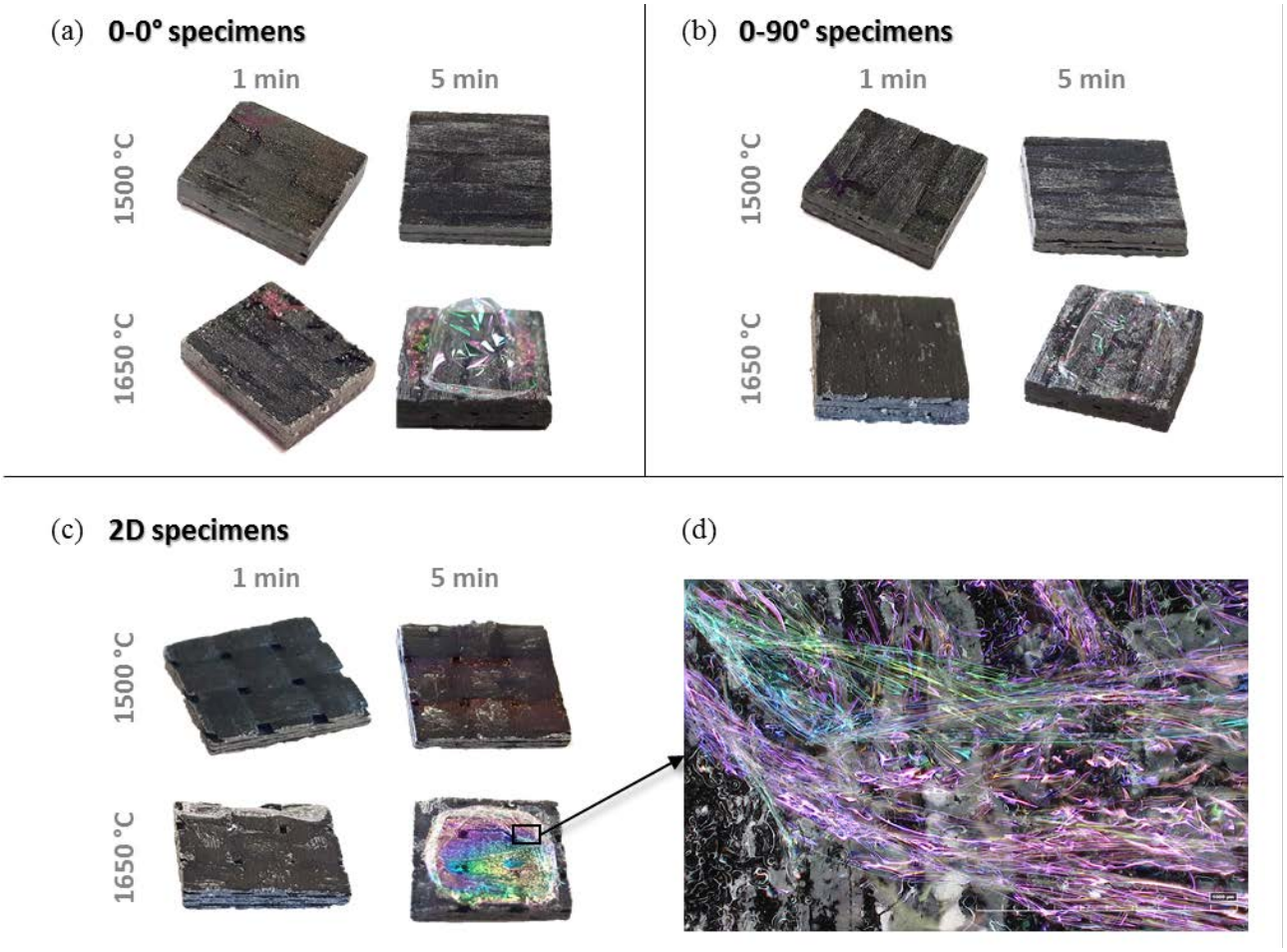

Figure 5. Appearance of the oxidized specimens after bottom loading furnace tests at 1500 °C and 1650 °C for 1 min and 5 min in air: (a) sample 0-0°, (b) sample 0-90° and (c) sample 2D. (d) Optical image detail of a soft iridescent glass bubble grown on the surface of the specimen shown in (c).

A way to evaluate the oxidation extent is the weight change (Table 3). However, it is important to point out that mass changes are the result of negative terms (carbon fibres oxidation and matrix decomposition in volatile species) and positive terms (formation of solid oxide scale). Although there are remarkable similarities between these materials and those reported in literature, (Table 1), the comparison among mass variations after oxidation tests is not often reliable due to testing conditions (e.g. time and temperature exposure, oxidizing environment, specimen dimensions). In literature, we can often find oxidation tests carried out under static air using a

muffle furnace or thermo-gravimetric analysis (TGA). The bottom loading furnace used to test the oxidation resistance of the composites in this study has the advantage to introduce the specimens when the target temperature is reached, avoiding further oxidation during heating ramp. However, during the introduction of the samples in the furnace, cold air enters the lower part of the chamber, heats up and causes a turbulent flow, leading to harsher conditions than those of a thermo-gravimetric analyser: Vinci et al. [30] reported that the exposure to air at 1500 °C for 1 min in the bottom loading furnace induced almost the same degree of oxidation of the equivalent TGA test carried out at 1550 °C for 2.5 h. In addition, the results are often not available or are expressed differently (e.g. weight loss percentage or mass variation normalized over to initial surface). For instance, H. Hu et al. [33] developed C/SiC material enriched with about 25 vol% ZrB_2 particles by PIP and studied the oxidation properties at 1200 °C in a muffle furnace; they reported a mass loss of 4.5% and 11.4% after oxidation for 20 min and 40 min, respectively. D. Huang et al. [36] evaluated the oxidation resistance of C/C-ZrB_2-ZrC-SiC composite under static air in a muffle furnace at 1100 °C up to 60 min; after 20 min the mass loss was no more than 1%, while after 60 min a mass loss of 10.96 % was reported.

Among sample 0-0°, 0-90° and 2D, the main differences were caused by the greater number of defects and rougher surface of 2D samples compared to the others. Weight loss was notably higher at 1650 °C than at 1500 °C. However, after an initial weight loss, the protective film acted as a barrier and the weight was nearly unchanged after 5 min exposure in air for all of the samples both at 1500 °C and 1650 °C (Table 3).

Vinci et al. [30] reported a range of weight loss from -1.9 to -3.6 mg/cm^2 testing similar materials in the same furnace at 1500 °C for 1 min. It is interesting to note that despite the content of ZrB_2 was higher than 46 vol%, it was not effective to reduce weight loss.

Table 3. Mass variations normalized to the surface area and average thickness of the oxidized layer after short oxidation tests at 1500 °C and 1650 °C for 1 min and 5 min of samples 0-0°, 0-90° and 2D.

	Exposure time (min)	Sample label 0-0°	0-90°	2D
Δm/S 1500 °C (mg/cm^2)	1	-2.9	-3.1	-5.1
	5	-1.6	-2.9	-4.9
Δm/S 1650 °C (mg/cm^2)	1	-11.6	-10.7	-7.6
	5	-12.3	-10.1	-8.3
Oxide thickness 1500 °C (μm)	1	~20	~21	~27
	5	~26	~26	~40
Oxide thickness 1650 °C (μm)	1	~30	~30	~43
	5	~32	~33	~46

In the following, the crystalline phases of tested samples were discussed. As example, in Fig. 6, X-ray diffraction patterns collected on the surface of the 0-0° specimens, after oxidation in air at 1500 °C and 1650 °C for 1 min and 5 min, were reported. The main crystalline phase was monoclinic ZrO_2 (PDF 65-1025) as product of ZrB_2 oxidation, that increased with the increase of time and oxidation temperature; trace amounts of tetragonal zirconia (PDF 88-1007) were detected only in XRD patterns after oxidation at 1500 °C. B_2O_3 was not detected in the surface layer; this could be attributed to its relatively low melting temperature (445 °C) [37] which leads to the formation of a glass. SiC(O) evolution was more difficult to track because of its surficial oxidation into glassy and crystalline SiO_2 (PDF 47-11449) [38]. The underlying SiC(O), not exposed to air, was subjected to crystallization into β-SiC (PDF 65-0360). After 5 min at 1650°C, XRD pattern of β-SiC is sharper than the pattern after 1 min at the same temperature. A similar trend, less marked, was detected at 1500°C. No reflections relative to carbon or carbides were observed for all the oxidized specimens. For all the oxidized composites peaks relative to ZrB_2 were still well visible. On the contrary, Vinci et al. [30] did not observe ZrB_2 reflections after oxidation of C/ZrB_2-SiC at 1500 °C and 1650 °C despite the initial higher content of ZrB_2 in the matrix, see Table 1. XRD patterns of samples 0-90° and 2D were mostly identical, with no relevant differences across the samples, and therefore they were not shown.

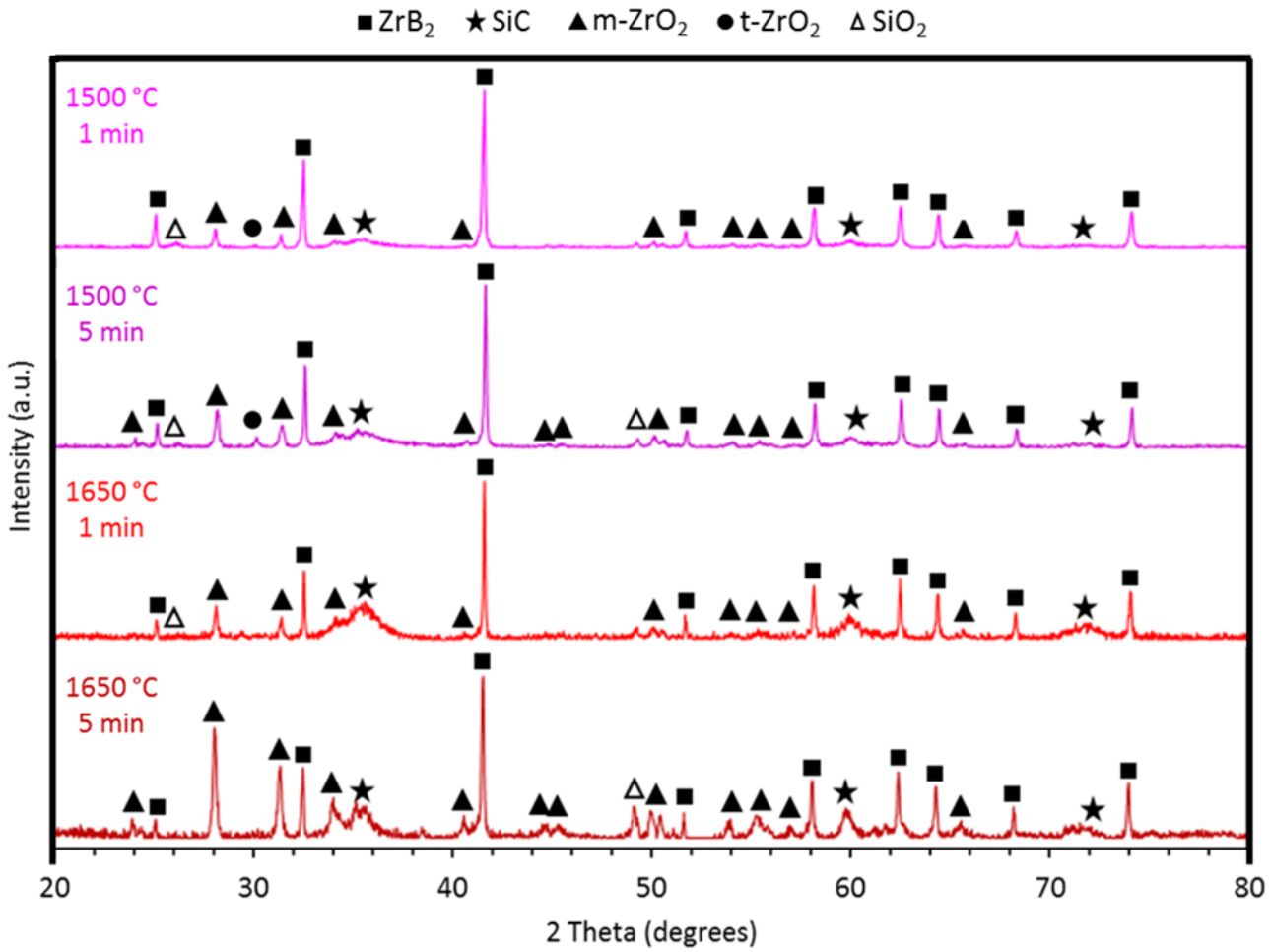

Figure 6. X-ray diffraction patterns collected on the surface of 0-0° specimens after oxidation at 1500 °C and 1650 °C in air for 1 min and 5 min.

Following the XRD investigation, SEM-EDS characterization was carried out on the surface and cross section of the oxidized samples. A typical top view of the surface of the specimens oxidized at 1500 °C and 1650 °C for 1 min and 5 min is shown in Fig. 7a-d, insets in Figures highlight the evolution of morphology of ZrO_2 grains with increasing time and temperature of the oxidation test.

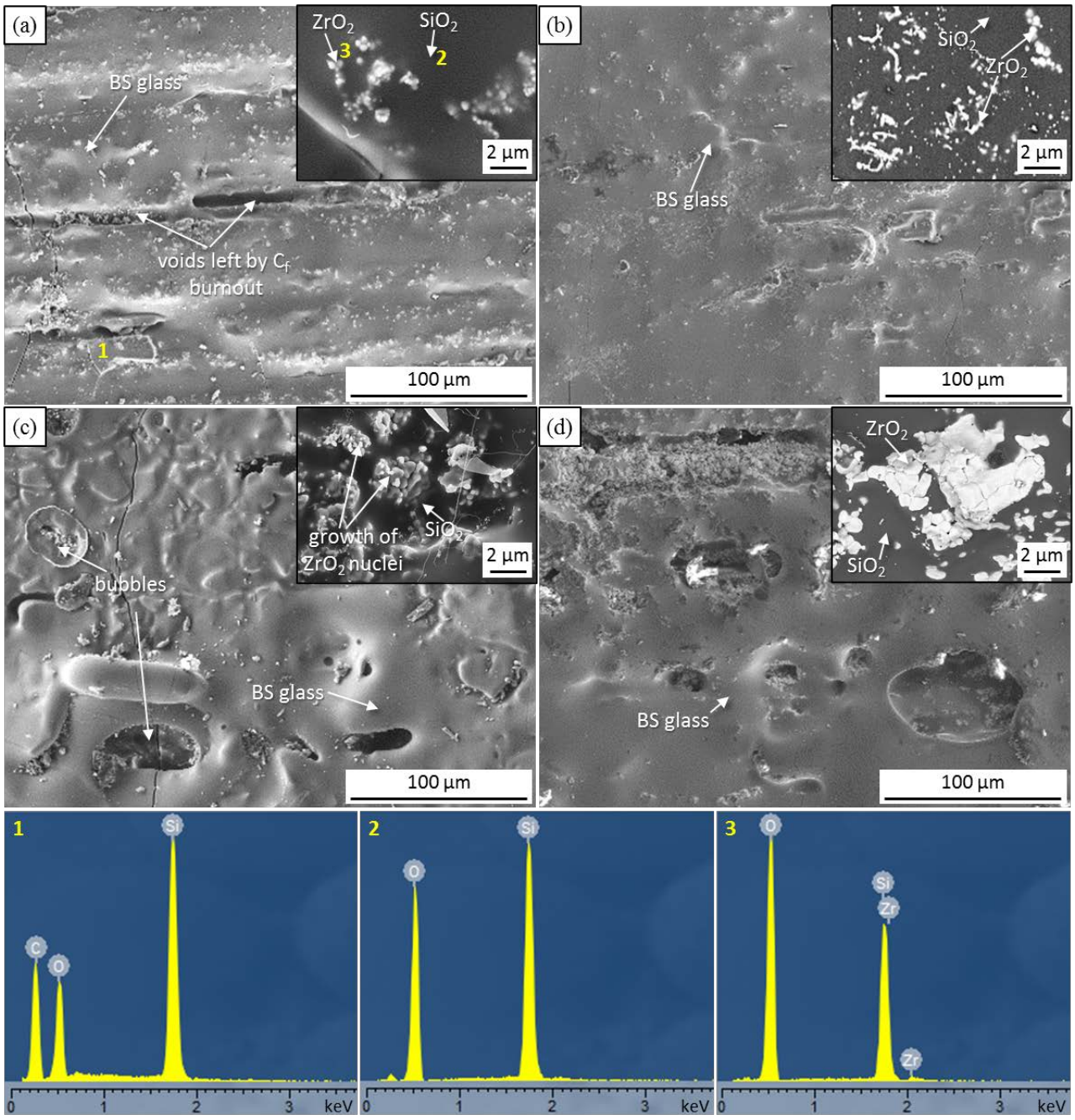

Figure 7. Top view of specimens (0-0° sample) oxidized in air in a bottom load furnace: at 1500 °C for (a) 1 min and (b) 5 min; at 1650 °C for (c) 1 min and (d) 5 min. Insets of the figures highlight the morphology of ZrO_2 grains embedded in the glass. At the bottom, EDS spectra of the phases as indicated.

As can be seen in Fig. 7a, after oxidation at 1500 °C for 1 min fibres onto or close to the surface were consumed and grooves are visible in their place. Tiny precipitated ZrO_2 crystals (bright phase) were found immersed into a borosilicate (BS) glass layer formed on the top. Oxidation at 1500 °C for 5 min induced the formation of a continuous BS glass scale which

homogeneously covered the surface, flowing in the grooves left by oxidized fibres, thus preventing further oxygen penetration inside the material (Fig. 7b). After oxidation at 1650 °C the surface appeared more damaged, a higher amount of blisters was observed and the whole surface became rougher (Fig. 7c,d). The great amount of liquid phase which spread from the subsurface towards the surface and the evolution of volatile oxides formed during oxidation led to bubble formation and rupturing. This in turn exposed the underlying bulk layer to oxygen again [30,39]. Further inspection on the ruptured bubbles showed islands of tiny ZrO_2 crystals in coral-like shape, in agreement with [30] (inset in Fig. 7c), due to the evolution of small nuclei in branches of a dendrite. Previously Karlsdottir et al. [40] called this type of dendritic zirconia as "secondary zirconia" and reported that it is dissolved in the boria–silica–zirconia liquid, thus crystals precipitated when the B_2O_3 evaporates. The number of blisters in the borosilicate glass scale increased with the exposure time at 1650 °C (Fig. 7d), precipitated ZrO_2 crystals underneath the ruptured bubbles increased in size and took on a rounded shape (inset in Fig. 7d). The surface of samples 0-90° and 2D was very similar to that reported in Fig. 7, so only the surface of the 0-0° sample was reported.

In supplementary information, see Fig. S1, the low magnification micrographs of the cross section of samples 0-0°, 0-90° and 2D after the four oxidation tests are presented. As an example, micrographs of the cross section of samples 0-0° oxidised at 1500 °C for 1 min are reported in Fig. 8a-e with the corresponding EDS spectra acquired in different spots, even though it was difficult to detect B_2O_3 by EDS, as boron is a light element [41].

Fig. 8a,b shows the cross section of the sample close to the top surface, which was not grinded after manufacturing to avoid interruption of fibres, while Fig. 8c shows the cross section of the specimen close to a machined side. As can be seen in Fig. 8a, the matrix underneath the top (orange dashed lines) was enriched of SiC(O) and SiO_2 (see EDS spectrum in Fig. 8).

A detail of partially filled holes left by carbon fibres oxidation is reported in Fig. 8b. It is worthy to note that ZrB_2 close to the surface appeared only partially oxidized, showing nano-crystals of ZrO_2 on the particle surface (Fig. 8c). In the cross section of a machined side (Fig. 8d), it is easier to

evaluate the thickness of the oxide scale. Hence, the modified layer thickness of the specimen was found in the range of 5-25 μm. Moving inwards in the oxidized scale, it was also possible to see a carbon fibre partially surrounded by BS glass film containing inclusions of ZrO_2, that could be considered a further mechanism of fibre protection toward oxidation (Fig. 8e).

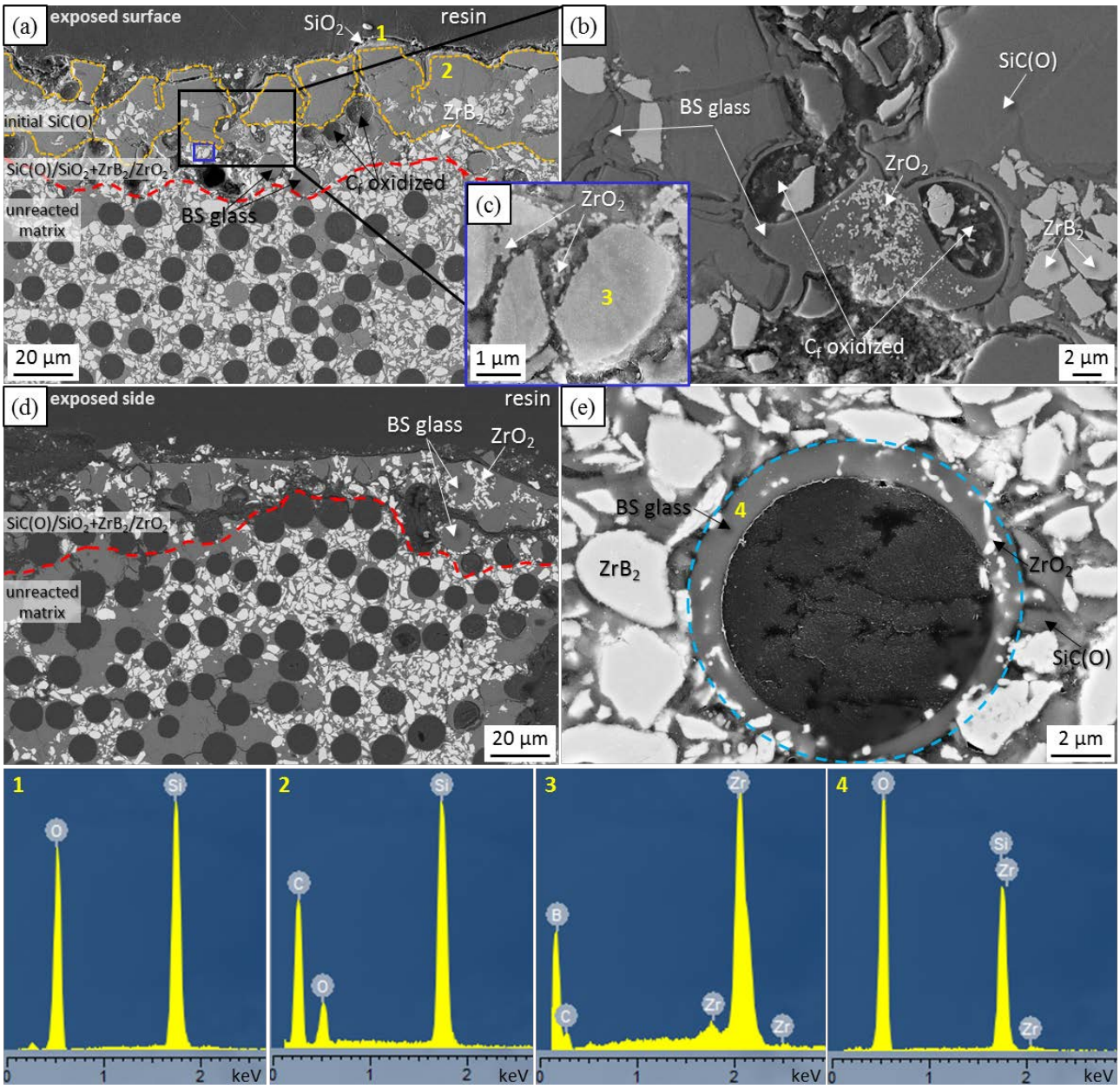

Figure 8. Polished cross section of the specimen (sample 0-0°) after short term oxidation test at 1500 °C for 1 min in air. (a) Micrograph of the exposed surface, SiC(O)-rich area, (b) magnification of the BS glass in the voids left by the C_f oxidation and (c) magnification of the partially oxidized ZrB_2 particles; (d) micrograph of the exposed side. (e) High magnification micrograph of a fibre where the oxidation stopped thanks to the BS glass (marked with blue circle) that surrounded it. In the bottom EDS spectra of the phases as numbered.

The morphology of the cross section after 5 min exposure at 1500 °C is shown in Fig. 9a-c. The outer part was composed by a compact scale of BS glass and solid inclusions (ZrO_2) with a thickness of ~26 μm (Fig. 9a). Despite the thickness of the oxide scale was found similar to the shorter oxidation test, the prolonged time of exposure to oxygen caused the almost complete conversion of surficial SiC(O) into SiO_2 and later into BS glass due to reaction with B_2O_3. High magnification micrographs showed many ridges consisting of a core of fine secondary ZrO_2 surrounded by glass [40] (Fig. 9b) and the progressive oxidation of ZrB_2 particles from the external surface towards the unreacted matrix (Fig. 9c).

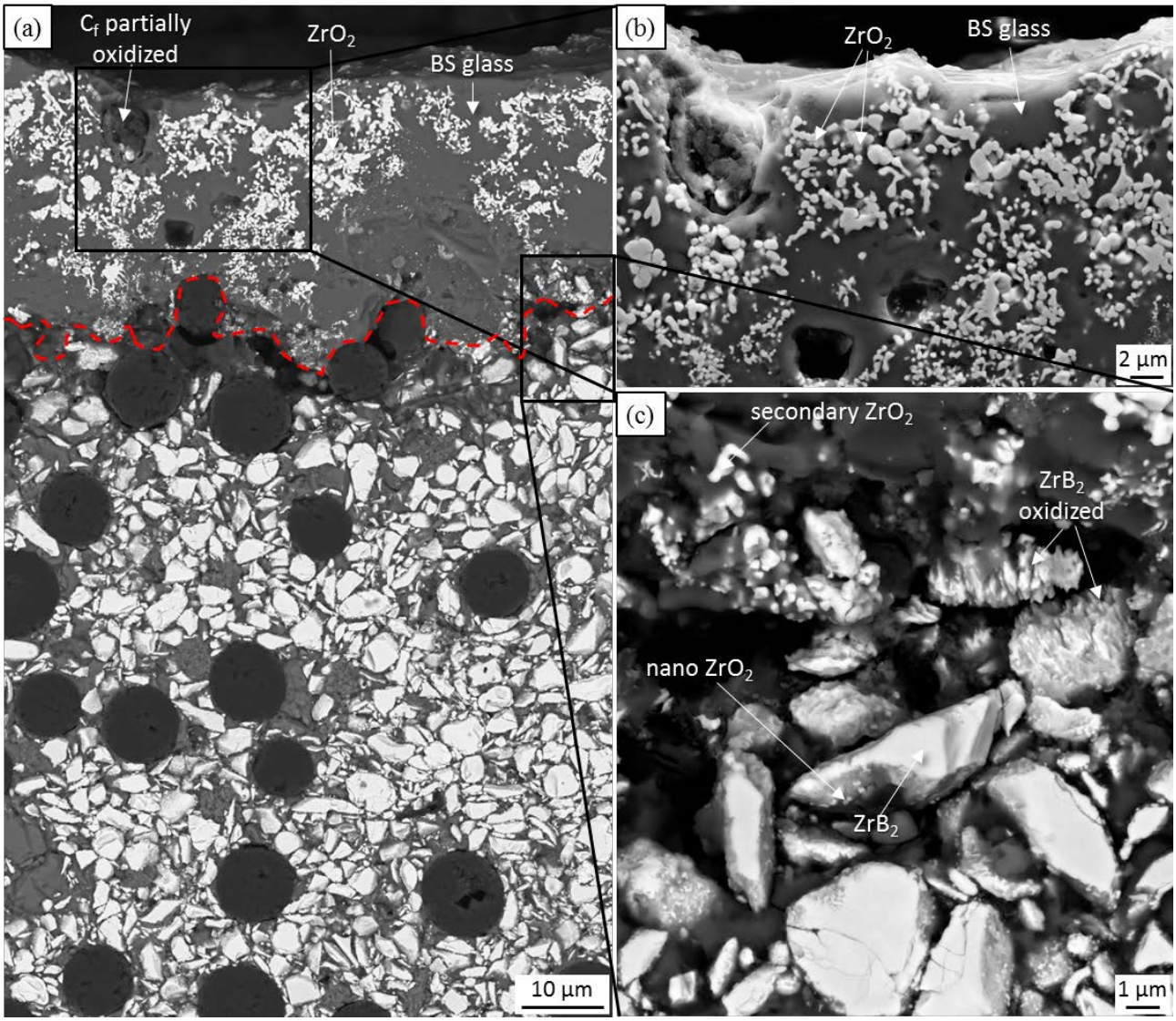

Figure 9. Polished cross section of specimen (sample 0-0°) after short term oxidation test at 1500 °C for 5 min in air: (a) overview of the microstructure, (b) magnification of the BS glass in which secondary ZrO_2 precipitates are embedded and (c) detail of ZrB_2 particles and progressive oxidation to ZrO_2 moving towards the top.

The microstructure of the cross section after oxidation at 1650 °C for 1 min is visible in Fig. 10a-d. In Fig. 10a, a layered structure is visible: an external borosilicate glass scale, an intermediate layer of ZrO_2/SiO_2 and an unreacted matrix layer. The coarsening of ZrO_2 grains is visible in Fig. 10b. A SiC-depleted layer between the ZrO_2/SiO_2 scale and the unreacted matrix was not detected. That region is commonly found in oxidized ZrB_2-SiC bulk ceramics, because of the active oxidation of SiC to volatile SiO [14,39]. Rezaie et al. [42] studied that graphite addition in a ZrB_2/SiC ceramic may affect the formation of this layer, as it promotes the preferential formation of $CO_{(g)}$. Hence, the lack of SiC-depleted region very likely depends on the high carbon fibre content.
Fig. 10c shows a SiC(O)-rich area, where the matrix damage was higher and oxygen could penetrate the sample to a depth of 55 μm. This observation is in agreement with ref. [43], where the cracked surficial SiC(O) acted as a preferential channel for oxygen diffusion trough the composite. Such SiC(O)-rich areas were found more prevalently in the sample 2D, (Fig. 2d), compared to samples 0-0° and 0-90°.
For the sake of comparison, in Fig. 10d, a cross section highlighting the lateral view of the fibres is shown. The micrograph captured the dynamics of two opposite mechanisms: the inward diffusion of the glassy phase through the channels and the evolution of volatile species that bubble through the molten glass. The oxidized thickness was calculated to be about 90 -150 μm.

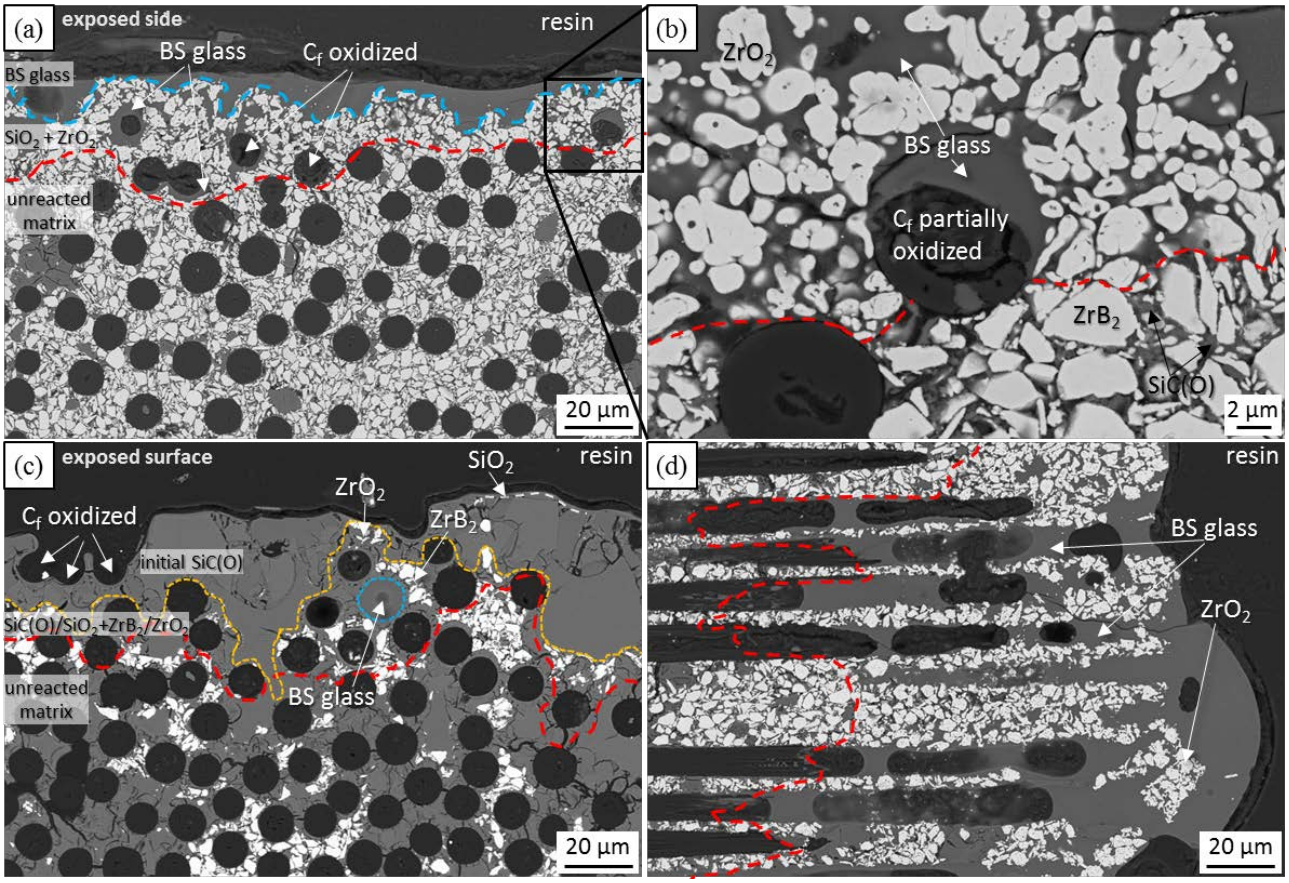

Figure 10. Polished cross section of specimen (sample 0-0°) after short term oxidation test at 1650 °C for 1 min in air: (a) micrograph of the exposed surface in a ZrB_2-rich area and (b) magnification of a partially oxidized fibre beneath the surface and the void filled by the BS glassy phase, (c) micrograph of the exposed surface in a SiC(O)-rich area, (d) lateral view of fibres.

The same microstructural features were observed after oxidation at 1650 °C for 5 min in air (Fig. 11a-e). A low magnification micrograph (Fig. 11a) shows that the specimens were not erode severely after 5 min exposure to air. The function of the borosilicate glass was evident in oxidized sections of the air exposed side (Fig. 11b), where the oxide thickness was around 25-35 µm (Table 3). Similarly to what was seen above (Fig. 10a,c), in regions with a higher amount of SiC(O), e.g. top of the specimens, the modified layer was thicker, up to 75 µm. In addition, the formation of a large BS glass bubble owing to the vigorous gas escape was reported in Fig. 11c. Partially attacked matrix and fibres were found underneath the oxide scale (Fig. 11d) and non oxidized bulk matrix and C_f (Fig. 11e) were reported to highlight the difference in microstructure.

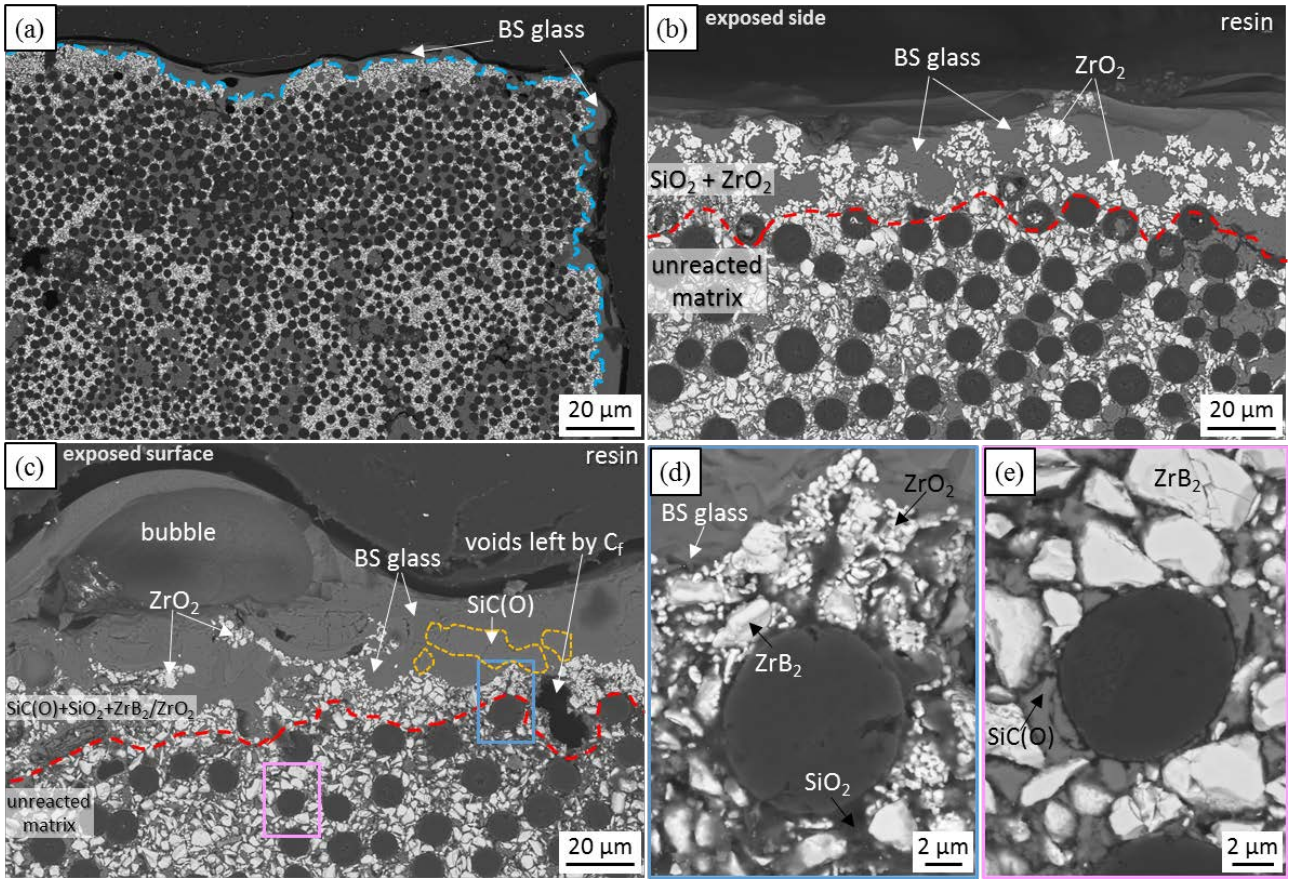

Figure 11. Polished cross section of specimen (sample 0-0°) after short term oxidation test at 1650 °C for 5 min in air: (a) low magnification micrograph of an edge exposed to air flow, (b) micrograph of the exposed surface in a ZrB_2-rich area and (c) micrograph of the exposed surface in a SiC(O)-rich area, showing oxidized thicknesses; high magnification micrographs of a fibre underneath the exposed surface surrounded by: a partially oxidized matrix (d), unreacted matrix (e).

In the supplementary information, Fig. S2, the cross sections of specimens are reported (sample 0-0°) after the four oxidation tests at the same magnification to have a comparison of the different oxide scale thickness in a glance.

Based on the above analysis, the main phenomena occurring during exposition of C/ZrB_2-SiC were: oxidation of carbon fibres on or close to the surface, oxidation of ZrB_2 to zirconia and boron oxide, oxidation of SiC to silica, formation of a borosilicate glass [29,30,32]. As described before, samples were introduced inside the hot chamber when the target temperature was reached, i.e. 1500 °C and 1650 °C. Opening the furnace the temperature slightly decreased, but in a few tens of seconds, the temperature was re-stabilized. Thus, all oxidation phenomena occurred almost

simultaneously. Although the permanence in the critical temperature range (700-1200 °C) [29] was rather short, near-surface fibres were still oxidized rapidly, and this contributed to an initial weight loss. However, the weight losses observed were much higher than expected and could be hardly attributed solely to that phenomenon or to the thin layer of oxide scale observed. The explanation could lie in the conversion of SiC(O) matrix into crystalline SiC, as it was obtained at the relatively mild condition of 1000 °C. Indeed, polymer-derived SiC(O) often contains free turbostratic carbon and terminal Si-CH_3 and Si-OH groups in case of incomplete pyrolysis [44]. Moreover, oxygen in polymer-derived SiC(O) reacts with carbon causing mass loss decomposing into SiO and CO gases via reaction 6 [45].

$$SiO_2 + C \rightarrow SiO + CO \quad (6)$$

According to the microstructural features of the specimens, the main mechanisms occurring in the UHTCMCs containing ZrB_2 particles embedded in amorphous SiC(O) are sketched in Fig. 12.

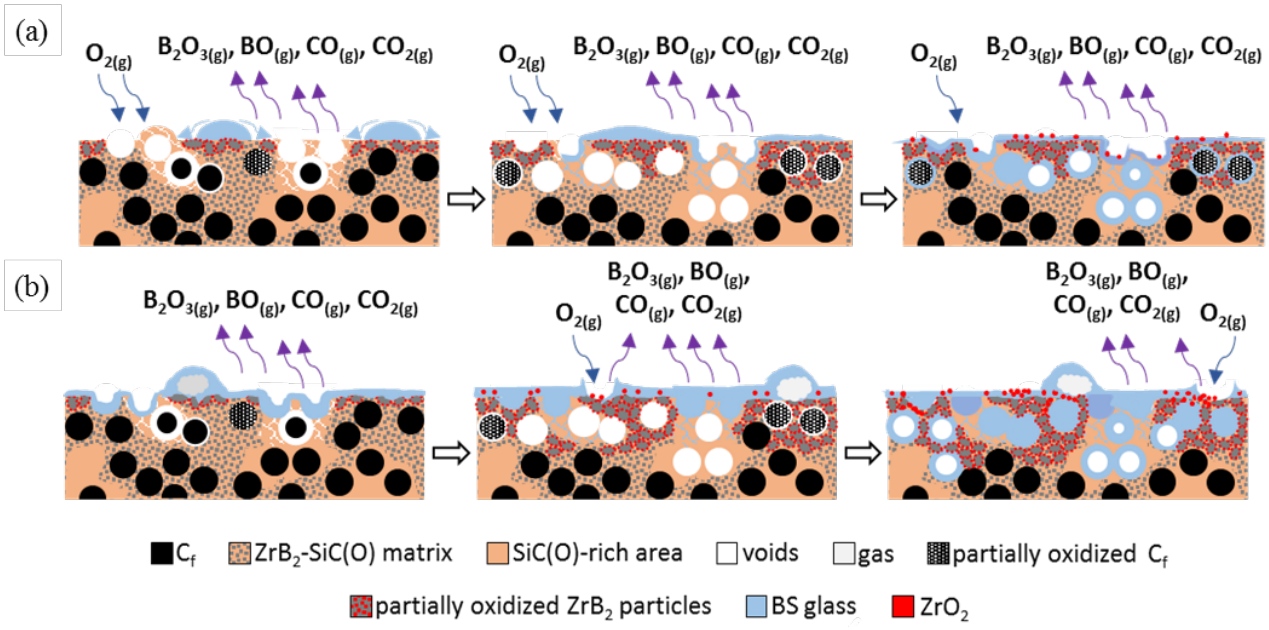

Figure 12. Sketch of oxidation mechanism of C_f/ZrB_2-SiC fabricated by water-based ZrB_2 powder slurry infiltration followed by 6 PIP cycles at (a) 1500 °C and (b) 1650 °C.

Yang et al. studied and comprehensively discussed the evolution of microstructure and properties of C/SiC composites prepared by PIP process after high-temperature oxidation. After oxidation in air at 1500 °C, the C/SiC composites were severely damaged, carbon fibres oxidation

and many microcracks were evident [4]. The same author tested PIP-C/SiC at 1600 °C, and the carbon fibres were completely consumed and SiC matrix became loose due to the escape of the gas phases produced beneath the surface [5]. The results obtained here indicate that the addition of ZrB_2 particles through a first cycle of slurry infiltration was essential for the formation of a borosilicate glassy layer, which played an important role in closing the holes left by carbon fibres oxidation and the cracks in the surface and subsurface layer.

Recent works concerning oxidation and ablation resistance of UHTCMCs have been discussed in ref. [46-48]. However, to the best of our knowledge, few works show the capability of protecting carbon fibres of a ZrB_2-SiC matrix obtained at mild conditions (i.e. 1000 °C). Moreover, it is interesting to compare the performance of the three samples analysed in this work with samples reported in ref [30-31], which were consolidated at stronger conditions (i.e. 1900 °C, 40 MPa). To this aim, the plot of Fig. 13a shows the oxide scale thickness after oxidation tests and carbon fibre content of samples while the plot of Fig. 13b shows density and the relative amounts of ZrB_2, SiC, C_f and porosity (normalized values) of samples. It can be clearly seen that from sample 0-0° to ZS10-55F the oxidation resistance is not strictly correlated to the increase of fibre content. However, in the case of sample Z40S-55F the amount of fibres (55 vol%) was too high to have a uniform coating by the matrix, resulting in poor resistance to oxidation, moreover the sample presents large ZrB_2-free matrix intra-bundle zones. The overall amount of SiC in the composite is also important to passivate the material surface. In samples Z10S-40F the presence of 6 vol% SiC promoted the formation of a borosilicate glass that diffused across the scale but efficacy is lower than in case of sample ZS20 and all of the samples of this work.

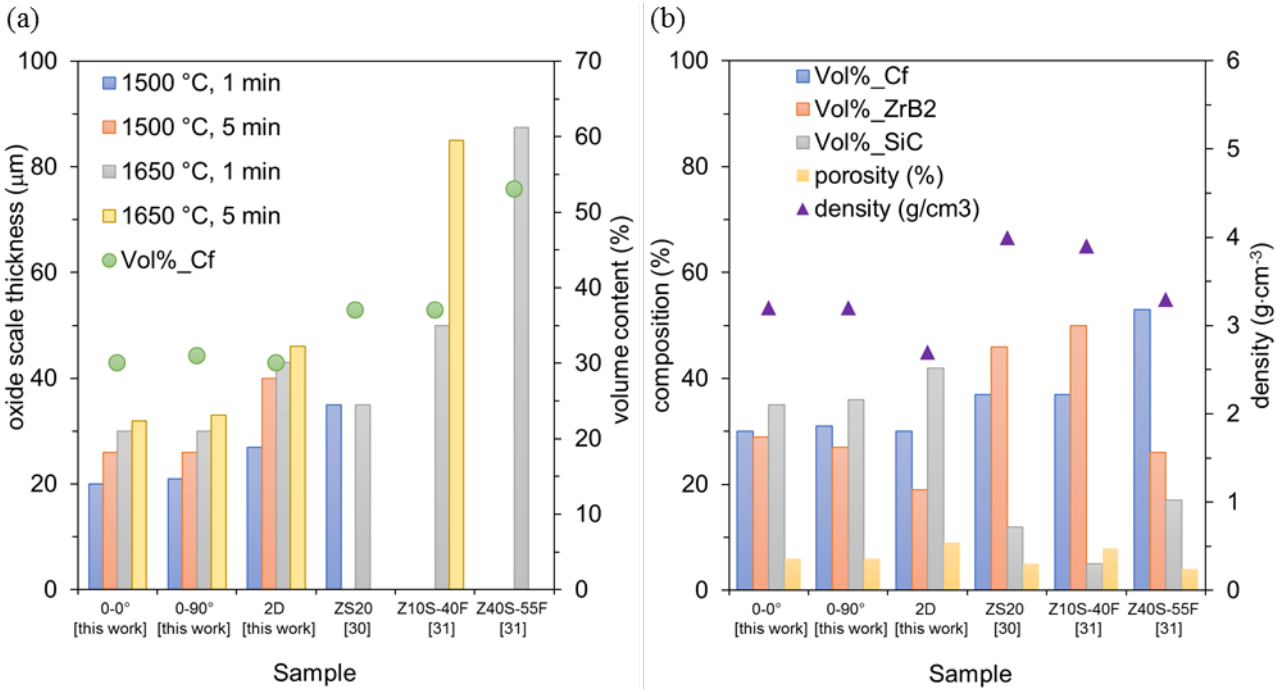

Fig. 13. Plots show (a) the volumetric content of fibre (Vol%_Cf) of samples and the thickness of the oxide scale after tests, (b) density and relative amounts of ZrB_2, SiC, C_f and porosity (normalized values) of the three samples of this work and three samples of ref. [30] and [31]. Unpublished data of the oxide scale thickness after tests at 1650 °C were reported for samples ZS10-40F and ZS40S-55F.

4. Conclusions

The oxidation behaviour of C_f/ZrB_2-SiC with different fibre architectures, manufactured by ZrB_2 powder slurry impregnation followed by SMP-10 infiltration and mild pyrolysis at 1000 °C, was investigated via TGA up to 1350 °C. The capability of the material to withstand the extreme harsh conditions was evaluated via short term oxidation tests in air at 1500 °C and 1650 °C in a bottom loading furnace for 1 min and 5 min. The exposure to high temperature in air activated the formation of a borosilicate glass, typical of ZrB_2-SiC binary systems, and it was found that a ZrB_2 content of 20-30 vol% of the matrix is able to impart a fast passivation. As expected, the oxidation resistance was affected by the distribution of ZrB_2 into the SiC matrix, highlighting the direct correlation between the oxide scale thickness and the quality of the slurry infiltration process. Independently of fibre architecture and complexity, the material hindered oxygen penetration within 5 min of exposure to air at high temperature.

Data availability statement

All data included in this study are available upon request by contact with the corresponding author.

Credit authorship contribution statement

F. Servadei: Investigation, Formal analysis, Data curation, Writing - original draft. L. Zoli: Conceptualization, Supervision, Methodology. A. Vinci: Writing - review & editing. P. Galizia: Supervision. D. Sciti: Project administration, Funding acquisition, Supervision, Writing - review & editing.

Declaration of Competing Interests

We declare that we have no financial and personal relationships with other people or organizations that can inappropriately influence our work, there is no professional or other personal interest of any nature or kind in any product, service and/or company that could be construed as influencing the position presented in, or the review of, the manuscript entitled “Significant improvement of the self-protection capability of ultra-high temperature ceramic matrix composites”.

Acknowledgements

The authors wish to thank A. Piancastelli, A. Natali Murri and C. Capiani for mercury intrusion porosimetry, thermogravimetric analysis and X-ray diffraction analysis, respectively.
This work was supported by the European Union’s Horizon 2020 “Research and innovation programme” [grant agreement No 685594].

Appendix A. Supplementary data

The following is Supplementary data to this article:

Download: Download Word document (809KB)

References

[1] W. Krenkel, Ceramic Matrix Composites, Wiley-VCH, Weinheim, 2008. https://doi.org/10.1002/9783527622412.

[2] S. Kumar, K.C. Shekar, B. Jana, L.M. Manocha, N. Eswara Prasad, C/C and C/SiC Composites for Aerospace Applications, in: N. Eswara Prasad, R. Wanhill (Eds.), Aerosp. Mater. Mater. Technol. Vol. 1 Aerosp. Mater. Indian Inst. Met. Ser., Springer, Singapore, Singapore, 2017: pp. 343–369. https://doi.org/10.1007/978-981-10-2134-3_15.

[3] B. Heidenreich, C/SiC and C/C-SiC Composites, in: P.B. Narottam, J. Lamon (Eds.), Ceram. Matrix Compos., John Wiley & Sons, Inc., Hoboken, NJ, USA, 2014: pp. 147–216. https://doi.org/10.1002/9781118832998.ch6.

[4] Y. Xiang, W. Li, S. Wang, Z.H. Chen, Oxidation behavior of oxidation protective coatings for PIP-C/SiC composites at 1500 °C, Ceram. Int. 38 (2012) 9–13. https://doi.org/10.1016/j.ceramint.2011.06.063.

[5] X. Yang, C. Feng, Z. hang Peng, W. Yi, G. de Li, Evolution of microstructure and mechanical properties of PIP-C/SiC composites after high-temperature oxidation, J. Asian Ceram. Soc. 5 (2017) 370–376. https://doi.org/10.1016/j.jascer.2017.07.001.

[6] Y. Wang, Z. Chen, S. Yu, Ablation behavior and mechanism analysis of C/SiC composites, J. Mater. Res. Technol. 5 (2016) 170–182. https://doi.org/10.1016/j.jmrt.2015.10.004.

[7] Y. Cui, A. Li, B. Li, X. Ma, R. Bai, W. Zhang, M. Ren, J. Sun, Microstructure and ablation mechanism of C/C-SiC composites, J. Eur. Ceram. Soc. 34 (2014) 171–177. https://doi.org/10.1016/j.jeurceramsoc.2013.08.026.

[8] B. Yan, Z. Chen, J. Zhu, J. Zhang, Y. Jiang, Effects of ablation at different regions in three-dimensional orthogonal C/SiC composites ablated by oxyacetylene torch at 1800 °C, J. Mater. Process. Technol. 209 (2009) 3438–3443. https://doi.org/10.1016/j.jmatprotec.2008.08.002.

[9] S. Tang, J. Deng, S. Wang, W. Liu, K. Yang, Ablation behaviors of ultra-high temperature ceramic composites, Mater. Sci. Eng. A. 465 (2007) 1–7. https://doi.org/10.1016/j.msea.2007.02.040.

[10] A. Cecere, R. Savino, C. Allouis, F. Monteverde, Heat transfer in ultra-high temperature advanced ceramics under high enthalpy arc-jet conditions, Int. J. Heat Mass Transf. 91 (2015) 747–755. https://doi.org/10.1016/j.ijheatmasstransfer.2015.08.029.

[11] M.M. Opeka, I.G. Talmy, E.J. Wuchina, J.A. Zaykoski, S.J. Causey, Mechanical, Thermal, and Oxidation Properties of Refractory Hafnium and zirconium Compounds, J. Eur. Ceram. Soc. 19 (1999) 2405–2414. https://doi.org/10.1016/S0955-2219(99)00129-6.

[12] S.R. Levine, E.J. Opila, M.C. Halbig, J.D. Kiser, M. Singh, J.A. Salem, Evaluation of ultra-high temperature ceramics for aeropropulsion use, J. Eur. Ceram. Soc. 22 (2002) 2757–2767. https://doi.org/10.1016/S0955-2219(02)00140-1.

[13] A.L. Chamberlain, W.G. Fahrenholtz, G.E. Hilmas, D.T. Ellerby, Characterization of zirconium diboride for thermal protection systems, Key Eng. Mater. 264–268 (2004) 493–496. https://doi.org/10.4028/www.scientific.net/kem.264-268.493.

[14] W.G. Fahrenholtz, G.E. Hilmas, I.G. Talmy, J.A. Zaykoski, Refractory diborides of zirconium and hafnium, J. Am. Ceram. Soc. 90 (2007) 1347–1364. https://doi.org/10.1111/j.1551-2916.2007.01583.x.

[15] W.G. Fahrenholtz, G.E. Hilmas, A.L. Chamberlain, J.W. Zimmermann, B. Fahrenholtz, Processing and characterization of ZrB2-based ultra-high temperature monolithic and fibrous monolithic ceramics, in: J. Mater. Sci., Springer, 2004: pp. 5951–5957. https://doi.org/10.1023/B:JMSC.0000041691.41116.bf.

[16] A. Rezaie, W.G. Fahrenholtz, G.E. Hilmas, Evolution of structure during the oxidation of zirconium diboride-silicon carbide in air up to 1500 °C, J. Eur. Ceram. Soc. 27 (2007) 2495–2501. https://doi.org/10.1016/j.jeurceramsoc.2006.10.012.

[17] W.G. Fahrenholtz, Thermodynamic analysis of ZrB_2-SiC oxidation: Formation of a SiC-

depleted region, J. Am. Ceram. Soc. 90 (2007) 143–148. https://doi.org/10.1111/j.1551-2916.2006.01329.x.

[18] R. Hassan, K. Balani, Oxidation kinetics of ZrB_2-and HfB_2-powders and their SiC reinforced composites, Corros. Sci, 177 (2020) 109024, https://doi.org/10.1016/j.corsci.2020.109024.

[19] E. Zapata-Solvas, D.D. Jayaseelan, P.M. Brown, W.E. Lee, Effect of La_2O_3 addition on long-term oxidation kinetics of ZrB_2-SiC and HfB2-SiC ultra-high temperature ceramics, J. Eur. Ceram. Soc. 34 (2014) 3535–3548. https://doi.org/10.1016/j.jeurceramsoc.2014.06.004.

[20] A. Paul, S. Venugopal, J.G.P. Binner, B. Vaidhyanathan, A.C.J. Heaton, P.M. Brown, UHTC-carbon fibre composites: Preparation, oxyacetylene torch testing and characterisation, J. Eur. Ceram. Soc. 33 (2013) 423–432. https://doi.org/10.1016/j.jeurceramsoc.2012.08.018.

[21] L. Silvestroni, D. Sciti, Densification of ZrB_2-$TaSi_2$ and HfB_2-$TaSi_2$ Ultra-High-Temperature Ceramic Composites, J. Am. Ceram. Soc. 94 (2011) 1920–1930. https://doi.org/10.1111/j.1551-2916.2010.04317.x.

[22] S. Zhu, W.G. Fahrenholtz, G.E. Hilmas, Influence of silicon carbide particle size on the microstructure and mechanical properties of zirconium diboride-silicon carbide ceramics, J. Eur. Ceram. Soc. 27 (2007) 2077–2083. https://doi.org/10.1016/j.jeurceramsoc.2006.07.003.

[23] K.S. Cissel, E. Opila, Oxygen diffusion mechanisms during high-temperature oxidation of ZrB_2 -SiC, J. Am. Ceram. Soc. 101 (2018) 1765–1779. https://doi.org/10.1111/jace.15298.

[24] H. Zhou, L. Gao, Z. Wang, S. Dong, ZrB_2 -SiC Oxidation Protective Coating on C/C Composites Prepared by Vapor Silicon Infiltration Process, J. Am. Ceram. Soc. 93 (2010) 915–919. https://doi.org/10.1111/j.1551-2916.2009.03481.x.

[25] O. Haibo, L. Cuiyan, H. Jianfeng, C. Liyun, F. Jie, L. Jing, X. Zhanwei, Self-healing ZrB_2–SiO_2 oxidation resistance coating for SiC coated carbon/carbon composites, Corros. Sci. 110 (2016) 265–272. https://doi.org/10.1016/j.corsci.2016.04.040.

[26] E.L. Corral, R.E. Loehman, Ultra-high-temperature ceramic coatings for oxidation protection of carbon-carbon composites, J. Am. Ceram. Soc. 91 (2008) 1495–1502.

https://doi.org/10.1111/j.1551-2916.2008.02331.x.

[27] S. Tang, J. Deng, S. Wang, W. Liu, Fabrication and Characterization of an Ultra-High-Temperature Carbon Fiber-Reinforced ZrB_2-SiC Matrix Composite, J. Am. Ceram. Soc. 90 (2007) 3320–3322. https://doi.org/10.1111/j.1551-2916.2007.01876.x.

[28] L. Liu, H. Li, W. Feng, X. Shi, K. Li, L. Guo, Ablation in different heat fluxes of C/C composites modified by ZrB_2-ZrC and ZrB_2-ZrC-SiC particles, Corros. Sci. 74 (2013) 159–167. https://doi.org/10.1016/j.corsci.2013.04.038.

[29] A. Vinci, L. Zoli, E. Landi, D. Sciti, Oxidation behaviour of a continuous carbon fibre reinforced ZrB_2–SiC composite, Corros. Sci. 123 (2017) 129–138. https://doi.org/10.1016/j.corsci.2017.04.012.

[30] A. Vinci, L. Zoli, D. Sciti, Influence of SiC content on the oxidation of carbon fibre reinforced ZrB_2/SiC composites at 1500 and 1650 °C in air, J. Eur. Ceram. Soc. 38 (2018) 3767–3776. https://doi.org/10.1016/j.jeurceramsoc.2018.04.064.

[31] L. Zoli, D. Sciti, Efficacy of a ZrB_2–SiC matrix in protecting C fibres from oxidation in novel UHTCMC materials, Mater. Des. 113 (2017) 207–213. https://doi.org/10.1016/j.matdes.2016.09.104.

[32] F. Servadei, L. Zoli, P. Galizia, A. Vinci, D. Sciti, Development of UHTCMCs via water based ZrB_2 powder slurry infiltration and polymer infiltration and pyrolysis, J. Eur. Ceram. Soc. 40 (2020) 5076–5084. https://doi.org/10.1016/j.jeurceramsoc.2020.05.054.

[33] H. Hu, Q. Wang, Z. Chen, C. Zhang, Y. Zhang, J. Wang, Preparation and characterization of C/SiC-ZrB_2 composites by precursor infiltration and pyrolysis process, Ceram. Int. 36 (2010) 1011–1016. https://doi.org/10.1016/j.ceramint.2009.11.015.

[34] Q. Li, S. Dong, Z. Wang, G. Shi, Fabrication and properties of 3-D Cf/ZrB_2-ZrC-SiC composites via polymer infiltration and pyrolysis, Ceram. Int. 39 (2013) 5937–5941. https://doi.org/10.1016/j.ceramint.2012.11.074.

[35] G. Chollon, Oxidation Behavior of Ceramic Fibers from the Si-C-N-O System and Sub-

Systems, Key Eng. Mater. 164–165 (1999) 395–398. https://doi.org/10.4028/www.scientific.net/kem.164-165.395.

[36] D. Huang, M. Zhang, Q. Huang, L. Wang, K. Tong, Mechanical Property, Oxidation and Ablation Resistance of C/C–ZrB_2–ZrC–SiC Composite Fabricated by Polymer Infiltration and Pyrolysis with Preform of Cf/ZrB_2, J. Mater. Sci. Technol. 33 (2017) 481–486. https://doi.org/10.1016/j.jmst.2016.09.003.

[37] Y.H. Seong, D.K. Kim, Oxidation behavior of ZrB_2-xSiC composites at 1500 °C under different oxygen partial pressures, Ceram. Int. 40 (2014) 15303–15311. https://doi.org/10.1016/j.ceramint.2014.07.036.

[38] D. Gao, Y. Zhang, J. Fu, C. Xu, Y. Song, X. Shi, Oxidation of zirconium diboride-silicon carbide ceramics under an oxygen partial pressure of 200Pa: Formation of zircon, Corros. Sci. 52 (2010) 3297–3303. https://doi.org/10.1016/j.corsci.2010.06.004.

[39] E. Opila, S. Levine, J. Lorincz, Oxidation of ZrB_2- And HfB_2-based ultra-high temperature ceramics: Effect of Ta additions, J. Mater. Sci. 39 (2004) 5969–5977. https://doi.org/10.1023/B:JMSC.0000041693.32531.d1.

[40] S.N. Karlsdottir, J.W. Halloran, A.N. Grundy, Zirconia transport by liquid convection during oxidation of zirconium diboride-silicon carbide, J. Am. Ceram. Soc. 91 (2008) 272–277. https://doi.org/10.1111/j.1551-2916.2007.02142.x.

[41] P.A. Williams, R. Sakidja, J.H. Perepezko, P. Ritt, Oxidation of ZrB_2-SiC ultra-high temperature composites over a wide range of SiC content, J. Eur. Ceram. Soc. 32 (2012) 3875–3883. https://doi.org/10.1016/j.jeurceramsoc.2012.05.021.

[42] A. Rezaie, W.G. Fahrenholtz, G.E. Hilmas, The effect of a graphite addition on oxidation of ZrB_2-SiC in air at 1500°C, J. Eur. Ceram. Soc. 33 (2013) 413–421. https://doi.org/10.1016/j.jeurceramsoc.2012.09.016.

[43] F. Uhlmann, C. Wilhelmi, S. Schmidt-Wimmer, S. Beyer, C. Badini, E. Padovano, Preparation and characterization of ZrB_2 and TaC containing C_f/SiC composites via Polymer-

Infiltration-Pyrolysis process, J. Eur. Ceram. Soc. 37 (2017) 1955–1960. https://doi.org/10.1016/j.jeurceramsoc.2016.12.048.

[44] G. Chollon, Oxidation behaviour of polymer-derived ceramics, in: P. Colombo and R. Riedel and G. D. Soraru and H.-J. Kleebe (Ed.), Polym. Deriv. Ceram. From Nano-Structure to Appl., DEStech Publications, 2010: pp. 292–308. 978-1-60595-000-6. ffhal-01374117f.

[45] Y. Hasegawa, K. Okamura, Synthesis of continuous silicon carbide fibre - Part 3 Pyrolysis process of polycarbosilane and structure of the products, J. Mater. Sci. 18 (1983) 3633–3648. https://doi.org/10.1007/BF00540736.

[46] A. Vinci, T. Reimer, L. Zoli, D. Sciti, Influence of pressure on the oxidation resistance of carbon fiber reinforced ZrB2/SiC composites at 2000 and 2200 °C, Corros. Sci., 184 (2021) 109377, https://doi.org/10.1016/j.corsci.2021.109377.

[47] J. Binner, M. Porter, B. Baker, J. Zou, V. Venkatachalam, V.R. Diaz, A. D'Angio, P. Ramanujam, T. Zhang, T.S.R.C. Murthy, Selection, processing, properties and applications of ultra-high temperature ceramic matrix composites, UHTCMCs–a review, Int. Mater. Rev. 0 (2019) 1–56. https://doi.org/10.1080/09506608.2019.1652006.

[48] S. Mungiguerra, G.D. Di Martino, A. Cecere, R. Savino, L. Silvestroni, A. Vinci, L. Zoli, D. Sciti, Arc-jet wind tunnel characterization of ultra-high-temperature ceramic matrix composites, Corros. Sci., 149 (2019) 18-28 https://doi.org/10.1016/j.corsci.2018.12.039.